Energy management of hybrid vehicles with state constraints: A penalty and implicit Hamiltonian minimization approach

Marcelino Sanchez Pantoja, Sebastien Delprat, Theo Hofman

Energy management of hybrid vehicles with state constraints: a penalty and implicit Hamiltonian minimization approach

Marcelino Sánchez[a,*], Sébastien Delprat[a], Theo Hofman[b]

[a] *Univ. Polytechnique Hauts-de-France, UMR 8201 - LAMIH, F-59313 Valenciennes, France.*
[b] *Eindhoven University of Technology, Department of Mechanical Engineering, Eindhoven 5600 MB, The Netherlands.*

Abstract

The energy management for hybrid electric vehicles can be seen as an optimal control problem. The Pontryagin's minimum principle represents a powerful methodology capable of solving the energy management offline. Moreover, the Pontryagin's minimum principle has been proved useful in the derivation of online energy management algorithms, such as the equivalent consumption minimization strategy. Nevertheless, difficulties on the application of the Pontryagin's minimum principle arise when state constraints are included in the definition of the problem. A possible solution is to combine the Pontryagin's minimum principle with a penalty function approach. This is done by adding functions to the Hamiltonian, which increase the value of the Hamiltonian whenever the optimal trajectory violates its constraints. However, the addition of penalty functions to the Hamiltonian makes it harder to compute its minimum. This work proposes an effective penalty approach through an implicit Hamiltonian minimization. The effectiveness of the approach is illustrated by obtaining the energy management for a hybrid electric vehicle modeled as a *mixed input-state constrained* optimal control problem. The dynamics considered for the energy management formulation are the battery state-of-energy and temperature.

Keywords: Energy management; Hybrid electric vehicles; Pontryagin's minimum principle; Mixed input-state constraints; Penalty function approach

1. Introduction

Hybrid electric vehicles (HEV) are one of the approaches aimed to reduce the dependency on finite fossil fuel resources used for transportation. Within an HEV, the power demand from the driver is split among the different powertrain energy sources in order to operate the internal combustion engine (ICE) in its most efficient region available, thus reducing the fuel consumption. The algorithm applied to achieve the best power split is known as energy management strategy (EMS) [1].

Although EMS mostly focusses on fuel efficiency, additional criteria may be considered as well, such as reducing the emission of pollutants [2, 3], improving the driver's comfort [4, 5], and prolonging the lifetime of the energy sources [6, 7]. Real-time EMS [8] are used to operate actual

*Corresponding author
Email addresses: Marcelino.SanchezPantoja@uphf.fr (Marcelino Sánchez), Sebastien.Delprat@uphf.fr (Sébastien Delprat), t.hofman@tue.nl (Theo Hofman)

cars and can only rely on causal algorithms. In simulation, finding the offline-EMS consists in computing (eventually, in a non-causal way) the ultimate performance of the HEV in order to compare different vehicle designs or to evaluate the performance of real-time EMS [9].

EMS in its most general form can be formulated as a mixed input-state constrained optimal control problem with discrete and continuous inputs and dynamics. The methods for solving this optimal control problem can be classified in three groups: dynamic programming (DP), *direct-approach* methods, and *indirect-approach* methods. The contribution of this work lies within the third group, the indirect-methods. However, a general discussion on the three groups of methods will be provided before entering into the details of the contribution.

In the DP approach, all the variables, inputs, states and time, are quantized. Then, the resulting discrete static optimization problem is solved to determine the optimal EMS. The DP approach is widely used in the literature, since it can solve the EMS in its most general form, i.e, with hybrid dynamics and input and state constraints. The main drawback of this method comes from its computational expensiveness, referred as the *curse of dimensionality* [10]. Namely, the number of elementary operations has an exponential relationship with respect to the number of states and inputs in the problem formulation. Likewise, the memory requirements increase exponentially with respect to the number of states. As a consequence, DP is, usually, restricted to problems with only one [11][12], or two continuous states [13].

In the *direct-approach* methods, only the time is often quantized (finite-time problems). The resulting static minimization problem is solved using mathematical programming techniques such as nonlinear programming, e.g., sequential quadratic programming (SQP) [14, 15], or convex programming, e.g., second-order cone programming (SOCP) [16], quadratic programming (QP) [17], and linear programming (LP) [18]. State constraints can be taken into account. Optimizing discrete controls leads to very large mixed-integer programming problems due to the considered long optimization horizon (typically, more than 1000 time steps). These problems are not tractable in general, even if they are restricted to be mixed-integer linear programming (MILP) problems. Nonetheless, when only continuous controls are considered, the direct approach does not posses the *curse of dimensionality* suffered by DP, therefore, it can be applied to obtain the optimal EMS, when several continuous states are considered. Moreover, it has been even applied to obtain, simultaneously, the optimal EMS and the optimal sizing of some components of the powertrain [19].

In the group of indirect methods, the calculus of variations or the Pontryagin minimum principle (PMP) is applied to obtain optimality conditions. The original EMS is then reduced to a simpler equivalent problem, namely, a boundary value problem (BVP). Hybrid-PMP [20, 21] allows considering both continuous and discrete systems, and thus, handling discrete controls signals, although they can lead to singular control issues [22]. State constraints lead to many theoretical difficulties, and there is no algorithm available to efficiently derive a solution in the general case. An algorithm is proposed in [23] to solve the EMS problem restricted to a single state.

Problems with many constrained states can be handled using the penalty function approach. It consists in adding an additional cost to the criterion that enforces the state to stay in the feasible region. This approach converts the state constrained problem into an unconstrained one that can be solved using the classical PMP [24, 25]. Nevertheless, the resulting optimality conditions are significantly more difficult to solve [26].

In this work, a novel method for the minimization of the Hamiltonian is proposed in order to overcome the difficulties of the penalty approaches to satisfy the optimality conditions. The novel

method is based on an implicit Hamiltonian minimization that, under strict convexity assumptions, can solve the EMS formulated with n states and m inputs under mixed input-state constraints. Although other penalty approaches have been successfully applied to the EMS under state constraints, they have been so far restricted to formulations with only one state [24, 25]. Increasing the number of states and inputs is relevant since it is necessary to produce a more accurate representation of the vehicle and all its subsystems that have an effect on the energy management. Preliminary results of this work were presented in [26].

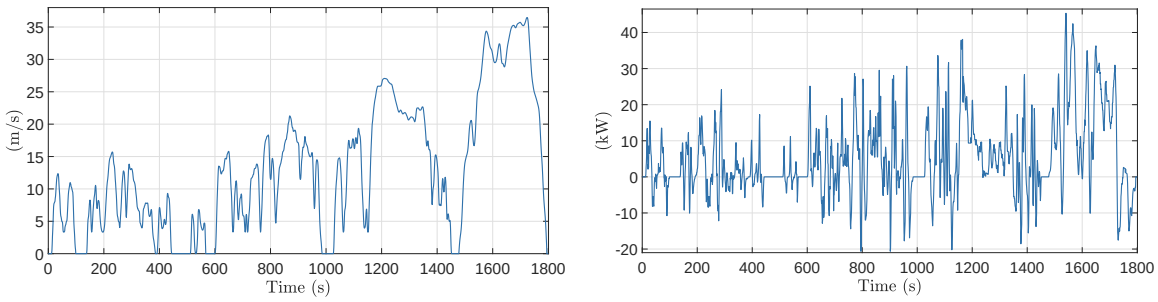

Figure 1: Worldwide Light-vehicle Test Cycle Class 3 (WLTC-C3) in m/s (left). Power demand signal $w(t)$ for the WLTC-C3 (right).

The the paper is organized as follows: Section II presents the vehicle modeling and the EMS formulation as an optimal control problem. The main results, an indirect-approach method based on penalty functions and an implicit Hamiltonian minimization, are presented in Section III. Section IV introduces algorithms to overcome numerical difficulties of the indirect-approach method. In Section V, the indirect-approach method is applied to compute the EMS formulated in Section II. At last, Section VI contains the conclusions and some perspectives on possible future work.

2. Problem statement

The hybrid vehicle EMS consists in computing the optimal power split between the different energy sources, when the vehicle is following a prescribed velocity profile, also known as driving cycle. An example of a driving cycle, the Worldwide Light-vehicle Test Cycle Class 3 (WLTC-C3), is depicted in Fig. 1 (left). For the considered series hybrid vehicle, see Fig. 2, the EMS input data is the power $w(t)$ (kW) required to propel the vehicle along the given driving cycle [1].

In the rest of this section, the offline-EMS will be defined in more detail for the considered series hybrid vehicle. However, it is worth noticing that the methodology presented in this work can be applied to many other hybrid vehicle topologies as well.

2.1. Series-HEV

Consider the HEV powertrain topology displayed in Fig. 2. The power required for propulsion at the input of the traction motor (TM), $w(t) \in \mathbb{R}$, must be provided at each instant by the auxiliary power unit (APU), $u(t) \in \mathbb{R}$, and/or the battery pack, $P_b(t) \in \mathbb{R}$. Moreover, the APU is subject to a on/off command signal, $\vartheta(t) \in \{0, 1\}$. The series topology imposes the following relationship among the power signals:

$$w(t) = \vartheta(t) \cdot u(t) + P_b(t). \tag{1}$$

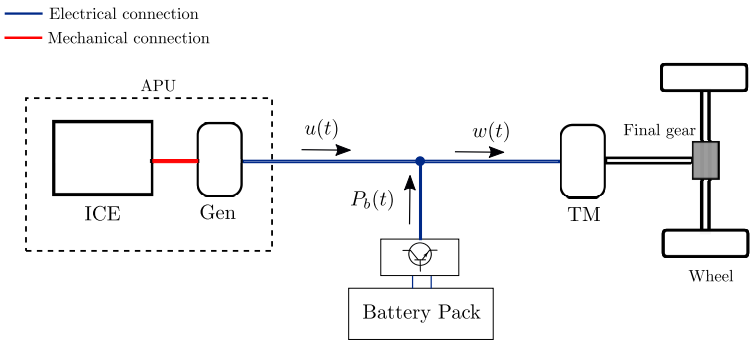

Figure 2: Diagram of the series-HEV powertrain.

The models required to compute $w(t)$, $P_b(t)$, and $u(t)$ are discussed in the following subsections. For the ease of readiness, in the following, the time dependence of the variables will be omitted when convenient.

2.1.1. Traction subsystem

The traction subsystem includes the vehicle model and transmission from the wheels to the TM. The corresponding model allows evaluating the energetic requirement of the vehicle. Given a velocity profile $v(t)$ and the vehicle parameters, the torque $T_w(t)$ and the angular velocity at the wheels $\omega_w(t)$, required to follow the driving cycle, are computed [1]:

$$T_w(t) = r_w\left(m_{eq}\cdot\frac{\mathrm{d}v(t)}{\mathrm{d}t} + m\cdot g\cdot c_r + \frac{1}{2}\rho_a\cdot A_f\cdot c_d\cdot v^2(t)\right), \tag{2}$$

$$\omega_w(t) = v(t)/r_w, \tag{3}$$

with c_r the tire rolling resistance (-), g the gravity acceleration $\left(\mathrm{kg}\cdot\mathrm{m/s^2}\right)$, ρ_a the air density $\left(\mathrm{kg/m^3}\right)$, A_f the vehicle frontal area $\left(\mathrm{m^2}\right)$, c_d the drag coefficient (-), γ the final gear ratio (-), r_w the radius of the wheels (m), m the vehicle mass (kg), and $m_{eq} = m + J_{tm}/\left(\gamma^2 r_w^2\right)$ the equivalent mass of the vehicle (kg). The vehicle is rear wheel driven (RWD): when braking, $T_w < 0$, only 40% of the torque is assumed to be provided by regenerative braking and the remaining 60% is assumed to be provided by the mechanical brakes. Indicated with $\mu_b(t)$ as a piecewise constant torque brake factor. A constant torque brake factor for regenerative braking is considered for the sake of simplicity. More advanced blending braking strategies may be applied, as in [27]. Finally, the TM torque and speed, denoted as T_{tm} and ω_{tm}, are derived:

$$T_{tm}(t) = \gamma\cdot\mu_b(t)\cdot T_w(t), \tag{4}$$

$$\mu_b(t) = \begin{cases} 0.4, & T_w(t) < 0 \\ 1, & \text{otherwise} \end{cases} \tag{5}$$

$$\omega_{tm}(t) = \omega_w(t)/\gamma. \tag{6}$$

At last, the power demand signal $w(t)$ is computed using the traction motor efficiency map η_{tm}:

$$w(t) = T_{tm}(t)\omega_{tm}(t)\eta_{tm}\left(T_{tm}(t),\omega_{tm}(t)\right)^{-sign(T_{tm}(t))} \tag{7}$$

Given the WLTC-C3 driving cycle, the power demand signal $w(t)$ is displayed in Fig. 1 (right).

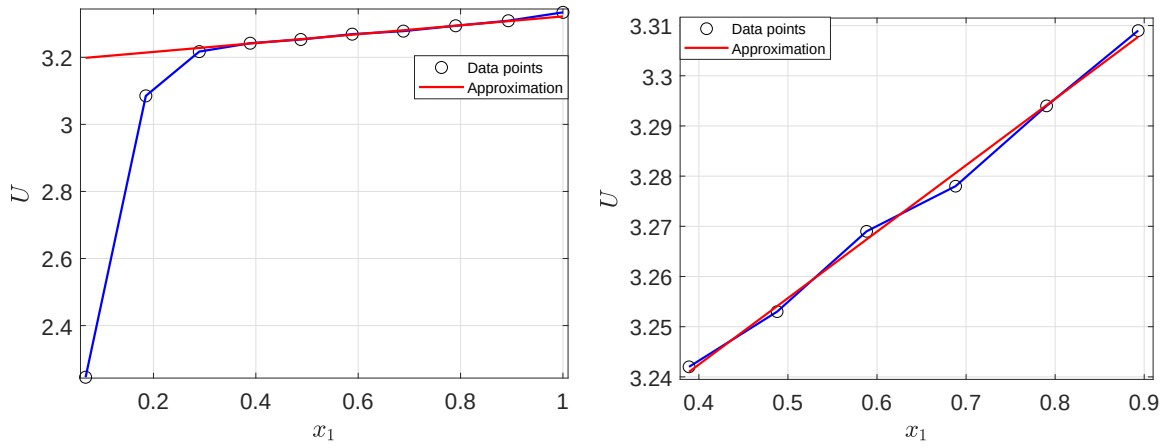

Figure 3: Open circuit voltage U as a function of x_1 derived from [29] (in blue) and the considered model $U(x_1) = a_{x_1} + b_{x_1} x_1$ (in red); plotted along the whole range of available data (left); plotted along the operating range (right). The parameters of $U(x_1)$ are $a_{x_1} = 27.14$ and $b_{x_1} = 653.85$.

2.1.2. Battery Pack

The battery pack is connected to a DC/DC converter that fixes the DC bus voltage. Its losses are assumed to be negligible. The energetic behavior is modeled using both the state-of-energy dynamics given in [17] and a thermal model similar to the one found in [28]. They relate the battery power, $P_b(t)$, to the state-of-energy, denoted as $x_1(t)$, and the battery temperature, denoted as $x_2(t)$. The battery state-of-energy, $x_1(t)$, is derived from an equivalent electric circuit model. It consists of an open circuit voltage $U(x_1(t))$ in series with a temperature dependent resistance $R_b(x_2(t))$. The state-of-energy, $x_1(t)$, has the following dynamics:

$$\dot{x}_1(t) = \frac{1}{\bar{U} \cdot Q} \left[-P_b(t) - \frac{R_b(x_2(t))}{U^2(x_1(t))} P_b^2(t) \right], \tag{8}$$

with $\bar{U}$ the maximum open circuit voltage (V) and Q the charge capacity of the battery pack (Ah). The battery state-of-energy, $x_1(t)$, is constrained between $\underline{x}_1$ and $\bar{x}_1$[1]

$$\underline{x}_1 \leq x_1(t) \leq \bar{x}_1. \tag{9}$$

Within the battery pack operating range (30%–90%), U is modeled as a linear function of x_1: $U(x_1) = a_{x_1} + b_{x_1} x_1$, derived from $LiFePO_4$ battery cell data found in [29], as shown in Fig. 3. The resistance R_b (Ω) is given by a linear function of x_2 (K).

The battery pack power $P_b(t)$ is constrained by the current limitations of the battery pack:

$$\underline{P}_b(R_b, U) \leq P_b(t) \leq \bar{P}_b(R_b, U), \tag{10}$$

with $\underline{P}_b = \underline{I} \cdot U - R_b \cdot \underline{I}^2$ and $\bar{P}_b = \bar{I} \cdot U - R_b \cdot \bar{I}^2$, $\underline{I}$ the minimum, and $\bar{I}$ the maximum battery pack current (A).

[1]Throughout the paper, an underline ($\_$) and an overline ($\bar{}$) are used to denote minimum and maximum value, respectively.

The dynamics of x_2 is obtained from a thermal balance energy equation [17, 28, 30, 31]:

$$\dot{x}_2(t) = \frac{1}{C_b}\left[h \cdot (T_\infty - x_2(t)) + \frac{R_b(x_2(t))}{U^2(x_1(t))} P_b^2(t)\right] \tag{11}$$

with C_b the heat capacity of the battery pack (kJ/K), T_∞ the ambient temperature (K), and h the heat transfer coefficient between the battery pack and its surroundings (W/K). The term depending on P_b stands for the heat dissipated by the battery resistance R_b. The battery resistance increases for low temperatures, thus reducing both the battery pack efficiency and the maximum power $\bar{P}_b$.

2.1.3. Auxiliary Power Unit

The APU consists of one ICE coupled with one generator (Gen) to produce electrical energy using fuel. The APU instantaneous fuel consumption, $\dot{m}_f(t)$ (g/s), required to generate a given electric power $u(t)$ (W), is estimated by the following quadratic function [17, 32]:

$$\dot{m}_f\left(u(t)\right) = a + b \cdot u(t) + c \cdot u^2(t). \tag{12}$$

The criterion to be minimized by the EMS is the total fuel consumption:

$$J = \int_0^{t_f} \left[\dot{m}_f\left(u(t)\right)\vartheta(t) + d \cdot (1 - \vartheta(t))\, u^2(t)\right] \mathrm{d}t, \tag{13}$$

where t_f stands for the duration of the driving cycle and d is a conversion factor $\left(\frac{\mathrm{g}}{(\mathrm{kW})^2 \cdot \mathrm{s}}\right)$. The additional term $(1-\vartheta)\cdot u^2$ allows enforcing $u = 0$, whenever $\vartheta = 0$ [26].

Optimizing the binary variable ϑ may lead to theoretical difficulties, such as singular controls [22] and non-unique optimal solutions. In order to keep the analysis simple enough and focus on the state constraints handling, the binary signal ϑ is assumed to be fixed beforehand. For instance, it can be computed using a set of empirical rules according to the power demand $w(t)$. The power produced by the APU is constrained by the physical limits of its components:

$$0 \leq u(t) \leq \bar{u}, \tag{14}$$

yet also by other components of the powertrain via (1):

$$w(t) - \bar{P}_b(t) \leq u(t) \leq w(t) - \underline{P}_b(t). \tag{15}$$

Constraints (14) and (15) can be combined together:

$$\begin{aligned} &\underline{u}'(t) \leq u(t) \leq \bar{u}'(t), \\ &\underline{u}'(t) = \max\left[0, w(t) - \bar{P}_b\right], \\ &\bar{u}'(t) = \min\left[\bar{u}, w(t) - \underline{P}_b\right]. \end{aligned} \tag{16}$$

2.2. Energy management as an optimal control problem

Over a known driving cycle, the energy management problem can be formulated as an optimal control problem (OCP) in the following way:

$$\min J(u) = \int_0^{t_f} \left[\vartheta \cdot \left(a + b \cdot u + c \cdot u^2\right) + d \cdot (1 - \vartheta) \cdot u^2\right] \mathrm{d}t, \tag{17a}$$

subject to:

$$\dot{x}_1(t) = \frac{1}{\bar{U} \cdot Q} \left[-(w - \vartheta u) - \frac{R_b(x_2)}{U^2(x_1)} (w - \vartheta u)^2\right], \tag{17b}$$

$$\dot{x}_2(t) = \frac{1}{C_b} \left[h \cdot (T_\infty - x_2) + \frac{R_b(x_2)}{U^2(x_1)} (w - \vartheta u)^2\right], \tag{17c}$$

$$\underline{u}'(t) \leq u(t) \leq \bar{u}'(t), \tag{17d}$$

$$\underline{u}'(t) = \max\left[0, w(t) - \bar{P}_b(t)\right],$$

$$\bar{u}'(t) = \min\left[\bar{u}, w(t) - \underline{P}_b(t)\right].$$

$$\underline{x}_1 \leq x_1(t) \leq \bar{x}_1, \tag{17e}$$

$$x_1(0) = x_{1,0}, \tag{17f}$$

$$x_2(0) = x_{2,0}, \tag{17g}$$

$$x_1(t_f) = x_{1,f}. \tag{17h}$$

The final condition $x_1(t_f)$ allows to guarantee that a certain amount of energy will remain in the battery at the end of the driving cycle. The final state-of-energy $x_1(t_f)$ is often assumed to be equal to $x_1(0)$ to allow a fair comparison with respect to the fuel consumption of conventional vehicles.

The problem statement above is a state and input constrained OCP formulation for the EMS. As it accounts for the battery thermal modeling, its solutions allows investigating the effect that a battery operating under *low-temperature* has on the fuel consumption.

3. Penalty function approach and implicit Hamiltonian minimization approach

This first part of this section explains how (17) can be solved through an equivalent unconstrained OCP by means of the penalty function approach. The second part explains how the PMP optimality conditions can transform the OCP formulation into an equivalent BVP. The optimal control must be chosen to minimize the Hamiltonian, a given scalar function. Due to the considered penalties, this minimization cannot be carried out explicitly. Hence, the last subsection focuses on an implicit minimization scheme.

3.1. Penalty function approach

In the penalty approach, the inequality constraints (17d) and (17e) are taken into account by extra terms, denoted as penalties, added to the cost functional (17a). These penalties drastically increase their values, whenever a constraint is violated or close to be violated. These characteristics force the optimal solution to satisfy the constraints. Consider a function P_z defined as follows:

$$P_z = P(z) = \begin{cases} (\underline{z} - z)^n, & z \leq \underline{z} \\ (z - \bar{z})^n, & z \geq \bar{z} \\ 0, & \text{otherwise.} \end{cases} \tag{18}$$

with $\underline{z}$ the minimum allowed value for z, $\bar{z}$ the maximum allowed value for z, and $n > 1$ a function parameter. P_z is known as an exterior penalty function, as it only affects the cost-functional when the constraints have been violated. Define P_u and P_x as the exterior penalty functions for the constraints (17d) and (17e), respectively, and $\tilde{P}_u = \phi \cdot P_u$, with $\phi = (1/\bar{u})^n$. Given (17a), the penalty approach solves (17) by solving an equivalent unconstrained-OCP:

$$\min \hat{J}(u) = \int_0^{t_f} \left[\vartheta \cdot \dot{m}_f(u) + d \cdot (1-\vartheta) \cdot u^2 + \frac{1}{\varepsilon} \left(\tilde{P}_u + P_x \right) \right] \mathrm{d}t, \tag{19a}$$

subject to:

$$(17\text{b}), (17\text{c}), (17\text{f}) - (17\text{h}), \tag{19b}$$

where ε is a real positive parameter pondering the penalty functions $\tilde{P}_u$ and P_x. If ε is small enough, the effect of $\tilde{P}_u$ and P_x increase to force the solution to (19), $\hat{J}^*$, to be approximately equal to the solution of (17), J^*. Moreover, $\hat{J}^* \to J^*$ as $\varepsilon \to 0$. Therefore, in order to get a fairly accurate approximation for the solution to (17), it is sufficient to solve (19) for a small enough value of ε. Proofs on the convergence of the penalty approach are given in [33, 34].

3.2. Optimality conditions

Necessary optimality conditions for (19) can be obtained from the PMP. Before discussing the PMP necessary conditions, it is necessary to define the Hamiltonian of the OCP, denoted as H. The Hamiltonian for (19) is given by:

$$H(u, x, \lambda | \vartheta, w) = \vartheta \cdot \dot{m}_f + d \cdot (1-\vartheta) \cdot u^2 + \frac{1}{\varepsilon} \left(\tilde{P}_u + P_x \right) + \lambda^T \dot{x} \tag{20}$$

with $\lambda(t) \in \mathbb{R}^2$ denoting the vector of co-states and $x = \begin{bmatrix} x_1 & x_2 \end{bmatrix}^T$ denoting the vector of states. The necessary conditions of optimality for (19) are the following [35]: (i) the optimal control, $u^*(t)$, minimizes the Hamiltonian for every possible control:

$$u^*(t) = \arg\min_{u \in \mathbb{R}} \{ H(u, x, \lambda \,|\, \vartheta, w) \}, \tag{21}$$

(ii) the co-states obey the following dynamics:

$$\dot{\lambda}_1(t) = -\frac{\partial H}{\partial x_1}, \tag{22}$$

$$\dot{\lambda}_2(t) = -\frac{\partial H}{\partial x_2}, \tag{23}$$

and (iii) the following final value condition for λ_2 is met:

$$\lambda_2(T) = 0. \tag{24}$$

It is not always possible to obtain u^* explicitly. Nevertheless, let us assume by now that an explicit expression can be computed for u^* and let us denote this expression as $\Pi(u, x, \lambda \,|\, \vartheta, w)$:

$$u^*(t) = \Pi(u, x, \lambda \,|\, \vartheta, w). \tag{25}$$

On the assumption that an optimal solution exists and that H satisfies the following sufficient strict convexity condition with respect to u:

$$\frac{\partial^2 H}{\partial u^2} > 0, \tag{26}$$

the conditions (21)-(24) become necessary and sufficient optimality conditions [36, 37]. Using (21)-(25), (19) can be formulated as an equivalent boundary value problem (BVP):

$$\dot{x}_1(t) = \frac{1}{\bar{U} \cdot Q}\left[-(w - \vartheta \cdot \Pi) - \frac{R_b(x_2)}{U^2(x_1)}(w - \vartheta \cdot \Pi)^2\right], \tag{27a}$$

$$\dot{x}_2(t) = \frac{1}{C_b}\left[h \cdot (T_\infty - x_2) + \frac{R_b(x_2)}{U^2(x_1)}(w - \vartheta \cdot \Pi)^2\right], \tag{27b}$$

$$\dot{\lambda}_1(t) = -\frac{1}{\varepsilon}\frac{\partial P_x}{\partial x_1}, \tag{27c}$$

$$\dot{\lambda}_2(t) = -\lambda_1 \frac{\partial \dot{x}_1}{\partial x_2} - \lambda_2 \frac{\partial \dot{x}_2}{\partial x_2}, \tag{27d}$$

$$\tag{27e}$$

$$\lambda_2(t_f) = 0, , \tag{27f}$$

$$(17f) - (17h). \tag{27g}$$

This BVP can be solved through different numerical methods, e.g. shooting, multiple-shooting, or collocation [38][39]. Due to its numerical stability, a collocation method is applied in this paper [39]. It is worth noticing that the use of penalty functions increases the difficulty for minimizing the Hamiltonian, which is a necessary optimality condition. A solution to overcome this issue is presented in the following subsection.

3.3. Implicit Hamiltonian minimization

Firstly, consider the minimization of the Hamiltonian with respect to the input signal: optimality condition (21). For an unconstrained input signal and assuming that H satisfies (26), the optimal control, $u^*(t)$, can be defined from the first order optimality conditions as follows:

$$u^*(t) = \left\{u(t) \,|\, \frac{\partial H\,(u, x, \lambda \,|\, \vartheta, w)}{\partial u(t)} = 0\right\}. \tag{28}$$

In general, (28) cannot be solved explicitly and an implicit Hamiltonian minimization can be used. Let us define $q(t)$ as follows:

$$q(t) = \frac{\partial H\,(u, x, \lambda \,|\, \vartheta, w)}{\partial u}, \tag{29}$$

The following equivalent conditions for $u^*(t)$ can be obtained:

$$q(0) = 0, \tag{30}$$

$$\dot{q}(t) = 0, \tag{31}$$

From (31), it follows:

$$\frac{\partial q}{\partial u}\dot{u} + \frac{\partial q}{\partial x_1}\dot{x}_1 + \frac{\partial q}{\partial x_2}\dot{x}_2 + \frac{\partial q}{\partial w}\dot{w} + \frac{\partial q}{\partial \vartheta}\dot{\vartheta} = 0,$$

from which the following optimal input dynamics can be computed:

$$\dot{u}^*(t) = \left(\frac{\partial q}{\partial u}\right)^{-1}\left(\frac{\partial q}{\partial x_1}\dot{x}_1 + \frac{\partial q}{\partial x_2}\dot{x}_2 + \frac{\partial q}{\partial w}\dot{w} + \frac{\partial q}{\partial \vartheta}\dot{\vartheta}\right), \tag{32}$$

Therefore, the explicit minimization of the Hamiltonian can be replaced by (30) and (32), since $\frac{\partial q}{\partial u} = \frac{\partial^2 H}{\partial u^2}$, (26) guarantees that $\left(\frac{\partial q}{\partial u}\right)^{-1}$ is defined. The methodology applied in order to approximate $\dot{w}$ and $\dot{\vartheta}$ is detailed in Appendix B. Considering these new optimality conditions, (19) can be solved via the following BVP [26]:

$$\dot{x}_1(t) = \frac{1}{\bar{U}\cdot Q}\left[-(w-\vartheta\cdot u^*) - \frac{R_b(x_2)}{U^2(x_1)}(w-\vartheta\cdot u^*)^2\right], \tag{33a}$$

$$\dot{x}_2(t) = \frac{1}{C_b}\left[h\cdot(T_\infty - x_2) + \frac{R_b(x_2)}{U^2(x_1)}(w-\vartheta\cdot u^*)^2\right], \tag{33b}$$

$$\dot{\lambda}_1(t) = -\frac{1}{\varepsilon}\frac{\partial P_x}{\partial x_1}, \tag{33c}$$

$$\dot{\lambda}_2(t) = -\lambda_1\frac{\partial \dot{x}_1}{\partial x_2} - \lambda_2\frac{\partial \dot{x}_2}{\partial x_2}, \tag{33d}$$

$$\dot{u}^*(t) = \left(\frac{\partial q}{\partial u}\right)^{-1}\left(\frac{\partial q}{\partial x_1}\dot{x}_1 + \frac{\partial q}{\partial x_2}\dot{x}_2 + \frac{\partial q}{\partial w}\dot{w} + \frac{\partial q}{\partial \vartheta}\dot{\vartheta}\right), \tag{33e}$$

$$q(0) = 0, \tag{33f}$$

$$(17\text{f}) - (17\text{h}), (27\text{f}), \tag{33g}$$

In the following, the solution to (33) will be denoted as $Y(t) = \left[x_1(t), x_2(t), \lambda_1(t), \lambda_2(t), u^*(t)\right]^T$. The dynamics of Y will be denoted as $F(Y,t)$. The idea of computing higher order time derivatives of the Hamiltonian was also considered in [40]. There, an inversion approach that allows parameterizing the OCP using only one higher-order unknown parameter is presented. However, for the inversion method to be applied an explicit expression for the optimal control is required, which is not the case for the problem formulation considered in this paper.

4. Numerical solution of the EMS

When the state-of-energy reaches a boundary, the co-state is discontinuous [41]. BVP solvers cannot easily handle such discontinuities straightforwardly. This section deals with the numerical details that need to be considered when trying to solve the BVP (33). The first two subsections discuss the *continuation procedure*, a numerical routine that breaks down the initial BVP into a sequence of several simpler sub-problems, starting from an unconstrained one down to a fully constrained one. Solutions to these sub-problems may temporarily exceed the state and control limits and as a result, the solutions may lay outside the definition domain of $F(Y,t)$. To deal with this issue, the third subsection proposes to extend $F(Y,t)$ outside its domain of definition.

4.1. Continuation Procedure

The numerical success of the BVP solver depends on the quality of the provided initial guess solution. The difficulty of generating a good enough initial guess is overcome by the implementation of a continuation or homotopy procedure [42, 43]. Before going into the application to the considered BVP, let us briefly recall how a continuation procedure is implemented in general.

Let us consider a BVP that depends on some parameters ζ. The objective is to compute a solution for the parameters values ζ_N using a BVP solver. The continuation procedure, depicted in the Algorithm 1, requires an initial guess Y_0 derived for some given parameter values ζ_0. At each iteration $i > 0$ of the continuation procedure, the solution Y_i of the BVP is numerically computed using Y_{i-1} as an initial guess. The parameters are varied smoothly from their initial value ζ_0 to their final values ζ_N. The performance of the algorithm depends on the number of steps N and the update function applied to vary the parameters from ζ_0 to ζ_N.

Algorithm 1: General continuation procedure

Inputs : ζ_0, Y_0, ζ_N, N;
Outputs: Y_N;
for $i = 1$ **to** N **do**
  $\zeta_i \leftarrow \text{update}\,(\zeta_{i-1})$;
  $Y_i \leftarrow \text{solve}\,(\zeta_i, Y_{i-1})$;
end

4.2. Application to the considered problem

In order to solve the BVP (33), first, an initial guess is generated and then several continuation procedures are used. In order to differentiate the parameters of each continuation procedure, the following notation is introduced: ζ_i^j denotes parameter values at iteration $i \in \{0, 1, \ldots, N\}$ of the continuation procedure described in step $j \in \{a, b, c\}$.

4.2.1. Step a: generation of an initial solution

The penalty pondering coefficient ε^a is initially set to a large value so the penalty functions are negligible. The initial co-states, $\left[\lambda_1(0),\ \lambda_2(0)\right]^T$ are selected such that assumption (26) is satisfied. Failing to meet this assumption could lead to $\frac{\partial^2 H}{\partial u^2} = \frac{\partial q}{\partial u}$ equal to zero, rendering the optimal control, (33e), undefined. Given (20), (26) is satisfied if $\lambda_2(0) \geq \frac{C_b}{U \cdot Q}\lambda_1(0)$. The corresponding initial optimal control $u(0)$ is numerically computed as a solution of $q(0) = 0$. Given these initial conditions, a solution is then numerically computed by integrating the differential equations (33a)-(33e) using an ODE solver. This solution is denoted by $Y^a(t) = \left[x_1^a(t), x_2^a(t), \lambda_1^a(t), \lambda_2^a(t), u^{*\,a}(t)\right]^T$.

4.2.2. Step b: First continuation procedure

The purpose of the first continuation procedure is to bring the final state-of-energy $x_1(t_f)$ to its prescribed final value $x_{1,f}$ and the second co-state final value $\lambda_2(t_f)$ to zero. The penalty pondering coefficient ε remains unchanged : $\varepsilon^b = \varepsilon^a$. The continuation procedure parameters are $\zeta^b = \left[x_1(t_f), \lambda_2(t_f)\right]^T$. ζ_0^b is set equal to the final conditions $\left[x_1^a(t_f), \lambda_2^a(t_f)\right]^T$ from the initial solution Y^a. ζ_N^b is set to $\left[x_{1,f}, 0\right]^T$ as defined in (17h) and (27f). The parameter update function is assumed linear, values of ζ_i^b are given by:

$$\zeta_i^b = \frac{\zeta_N^b - \zeta_0^b}{N^b} + \zeta_{i-1}^b, \tag{34}$$

The output of the continuation procedure is the unconstrained solution to (17). The continuation procedure is summarized in Algorithm 2.

Algorithm 2: First continuation procedure.

Inputs : $\zeta_0^b = \left[x_1^a(t_f), \lambda_2^a(t_f)\right]^T, Y_0^b = Y^a, \zeta_N^b = \left[x_{1,f}, 0\right]^T, N^b;$
Outputs: $Y_N^b;$

```
for i = 1 to N^b do
    ζ_i^b ← (ζ_N^b − ζ_0^b) /N^b + ζ_{i−1}^b ;
    Y_i^b ← solve (ζ_i^b, Y_{i−1}^b) ;
end
```

4.2.3. Step c: Second continuation procedure

The second continuation procedure activates the penalty functions by reducing the value of ε, thus $\zeta^c = \varepsilon$. ζ_0^c is set equal to the large value of ε used initially: $\zeta_0^c = \varepsilon^b = \varepsilon^a$. In order to obtain a solution that fulfills the constraints, a very small value of ε should be reached at the end of this continuation procedure : $\zeta_N^c \approx 0$. The values of ζ_i^c are chosen to be varied exponentially. The continuation procedure can be summarized in the following algorithm:

Algorithm 3: Second continuation procedure.

Inputs : $\zeta_0^c, Y_0^c = Y_N^b, \zeta_N^c = 1 \cdot 10^{-9}, N^c;$
Outputs: $Y_N^c;$

```
α ← (ln(ζ_N^c) − ln(ζ_0^c)) /N^c ;
for i = 1 to N^c do
    ζ_i^c ← e^α · ζ_{i−1}^c ;
    Y_i^c ← solve (ζ_i^c, Y_{i−1}^c) ;
end
```

The output of the second continuation procedure is the solution to constrained BVP (33). The general numerical procedure presented in this subsection is summarized in Fig. 4.

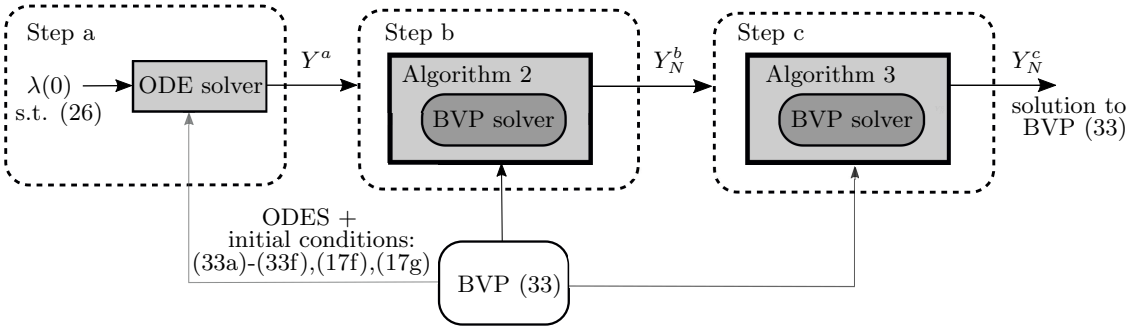

Figure 4: Overview of *Step a*, *Step b*, and *Step c*.

4.3. Function extension

The dynamics $F(Y,t)$ is not defined for $U(x_1) = 0$ due to the term of $1/U(x_1)$ in (8) and (11). As the only constraint for the initial co-states, used to generate the initial solution in *Step a*, is to satisfy (26), the states may reach values outside the definition domain of F. As a consequence,

Step a and *b* may not be feasible. Moreover, even in *Step c*, the BVP solver may require to evaluate $F(Y,t)$ outside its definition domain. To overcome the latter problems, $F(Y,t)$ is extended outside its definition domain and the resulting function is denoted by $F_{\text{ext}}(Y,t) \in \mathbb{R}^5$. F and F_{ext} are identical for all $Y \in Y_{\text{feas}}$. F_{ext} is obtained by replacing $f(x_1) = 1/U(x_1) : (-a_{x_1}/b_{x_1}, +\infty] \to \mathbb{R}^+$ by $f_{\text{ext}}(x_1 \,|\, \tilde{x}_1) : \mathbb{R} \to \mathbb{R}^+$, with:

$$f_{\text{ext}}(x_1 \,|\, \tilde{x}_1) = \begin{cases} 1/U(x_1), & \text{if } x_1 \geq \tilde{x}_1 \\ g(x_1), & \text{otherwise} \end{cases} \tag{35}$$

$$\begin{aligned} g(x_1) =& 1/U(\tilde{x}_1) + (x_1 - \tilde{x}_1)\frac{\mathrm{d}\,(1/U(x_1))}{\mathrm{d}x_1} + \\ & \frac{1}{2}(x_1 - \tilde{x}_1)^2 \frac{\mathrm{d}^2\,(1/U(x_1))}{\mathrm{d}x_1^2}, \end{aligned} \tag{36}$$

where $\tilde{x}_1$ is a scalar to be chosen from the interval $(-a_{x_1}/b_{x_1}, \underline{x}_1]$.

This extension is based on the Taylor series expansion and its generalization to terms depending on $n \in \mathbb{N}$ variables is given in Appendix A.

The Taylor-based function extension (35)-(36) preserves the convexity properties of the original function and thus guarantees that the Hamiltonian satisfies (26), which in turn guarantees that the solution remains unique and that (33e) is well defined. Choosing $\tilde{x}_1 = \underline{x}_1 = 0.1$, $1/U(x_1)$ and $f_{ext}(x_1 \,|\, \tilde{x}_1)$ are shown in Fig. 5 along with $x_1 = -a_{x_1}/b_{x_1}$, the limit of the definition domain for $1/U(x_1)$.

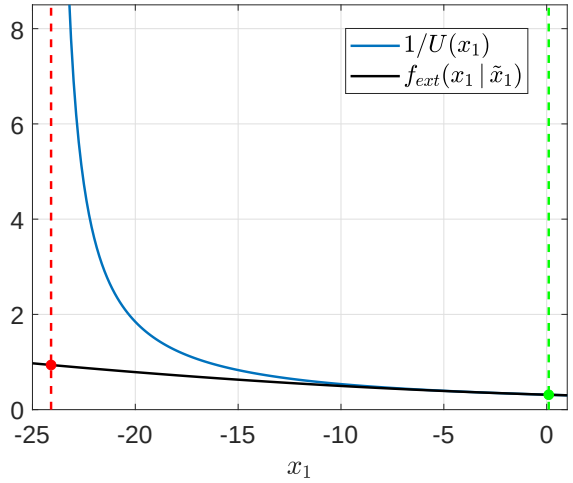

Figure 5: $1/U(x_1)$ (blue line), its function extension $f_{ext}(x_1 \,|\, \tilde{x}_1)$ (black line), the limit of the definition domain of $1/U(x_1)$: $x_1 = -a_{x_1}/b_{x_1}$ (red dotted line), and $\tilde{x}_1 = \underline{x}_1 = 0.1$ (green dotted line).

5. Numerical Results

Considering the vehicle parameters contained in Table 1, the offline-EMS is solved under *low-temperature* and *warm* operation conditions in order to study the effect of the battery temperature on the fuel consumption.

Parameter	Value	Units
M_{eq}	2166	kg
A_f	1.98	m^2
c_d	0.32	-
c_r	0.01	-
γ	4.2	-
r_w	0.26	m
g	9.81	kg·m/s^2
J_{tm}	0.045	kg·m^2
$\underline{I}$	-40	A
$\bar{I}$	40	A
a_{x_1}	653.85	V
b_{x_1}	27.14	V
Q	1800	A·s
h	4.343	W/K
C_b	142.56	kJ/K
a	0.2924	g/s
b	0.0834	$\frac{g}{kW \cdot s}$
c	0.0055	$\frac{g}{(kW)^2 \cdot s}$
d	1	$\frac{g}{(kW)^2 \cdot s}$
$\bar{u}$	17.5	kW

Table 1: Parameters considered in the numerical experiments.

5.1. Low-temperature operation

The *low-temperature* operation is defined here as starting the vehicle with $T_\infty = 253.15$ K (-20 °C), where T_∞ is assumed to remain constant along the entire driving cycle. At the beginning of the driving cycle, the following assumption holds: $x_2 = T_\infty$. Considering the WLTC-C3 driving cycle, the optimal offline-EMS defined in (17) is solved via the equivalent BVP (33) using a collocation solver [39] and the numerical procedure and function extension described in Section IV.

First, the initial guess Y^a is generated as described in *Step a* using $\lambda(0) = \begin{bmatrix} 1.4 \cdot 10^5 & 1.45 \cdot 10^5 \end{bmatrix}^T$ and the initial penalty pondering coefficient $\varepsilon^a = 1 \cdot 10^{12}$. The obtained initial solution Y^a is depicted in Fig. 6. The state-of-energy reaches negative values, showing that the initial guess does not necessarily have a physical meaning.

The final conditions from Y^a, $\begin{bmatrix} x_1^a(t_f), \lambda_2^a(t_f) \end{bmatrix}^T = \begin{bmatrix} -7.3, 5.32 \cdot 10^6 \end{bmatrix}^T$, are applied at the beginning of *Step b*: $\zeta_0^b = \begin{bmatrix} x_1^a(t_f), \lambda_2^a(t_f) \end{bmatrix}^T$. *Step b* allows computing a solution that reaches the expected

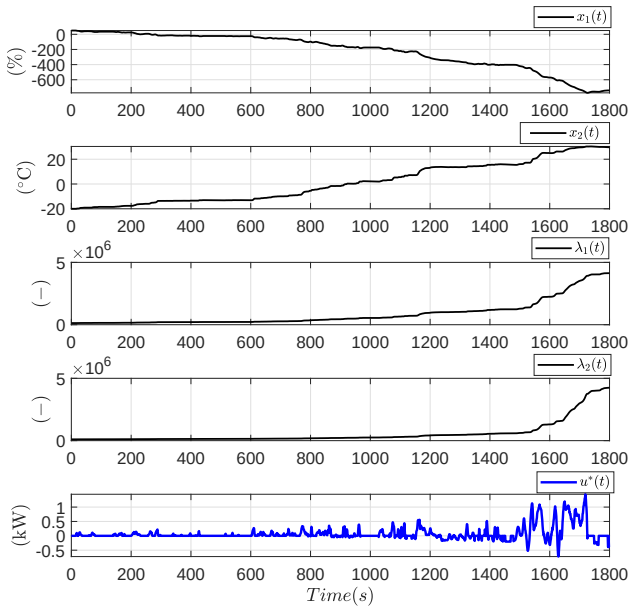

Figure 6: Initial guess Y^a generated in *Step a* for the WLTC-C3 driving cycle.

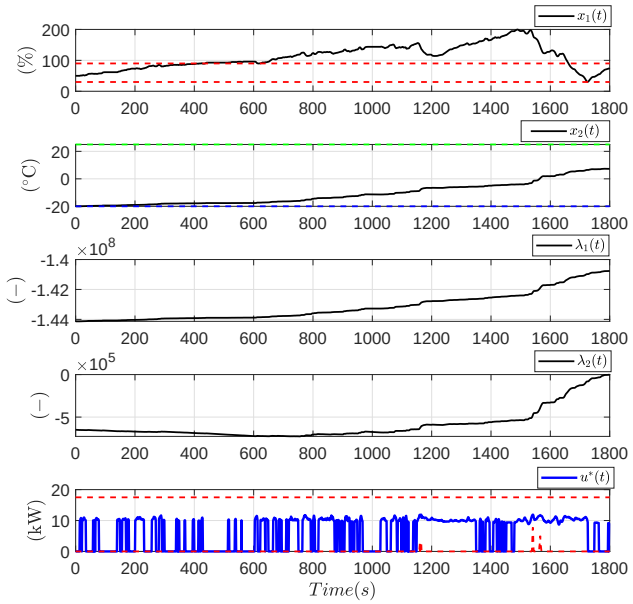

Figure 7: Unconstrained solution to (17) for the *low-temperature* operation and the WLTC-C3 driving cycle. The fuel consumption is 9.53 L/100 km. The dashed lines at the top and bottom subfigures represent the bounds on the state-of-energy and the control input, (17e) and (17d), respectively.

final state-of-energy and the necessary final condition for the second co-state: $\zeta_f^b = [x_1(t_f), 0]^T$. Its output Y_N^b, shown in Fig. 7, is the solution to EMS (17) without constraints, since the penalty functions are negligible: $\varepsilon^b = \varepsilon^a = 1 \cdot 10^{12}$.

The output of *Step b*, Y_N^b, is fed into *Step c*: $Y_0^c = Y_N^b$. *Step c* is used to activate the penalty functions. The initial penalty pondering coefficient is set to the same value of *Step b*:

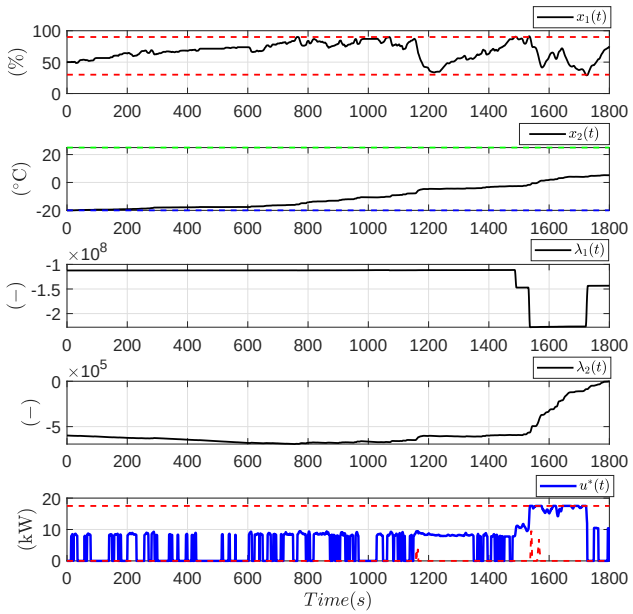

Figure 8: Constrained solution to (17) for the *low-temperature* operation and the WLTC-C3 driving cycle. The fuel consumption is 9.85 L/100 km. The dashed lines at the top and bottom subfigures represent the bounds on the state-of-energy and the control input, (17e) and (17d), respectively.

$\zeta_0^c = \varepsilon_0^c = \varepsilon^b = 1 \cdot 10^{12}$. The final penalty pondering coefficient is set to a small positive value: $\varepsilon_N^c = 1 \cdot 10^{-9}$. The output of *Step c*, Y_N^c, is the solution to constrained EMS (17) and is shown in Fig. 8. It allows computing the fuel consumption for the *low-temperature* operation : 9.85 L/100 km.

The constrained solution for the EMS, Fig. 8, shows a discontinuity phenomenon for $\lambda_1(t)$. This phenomenon is to be expected, whenever a state makes contact with its bounds [41]. It is worth noticing that the procedure proposed in this work does not require any *a priori* knowledge about these discontinuities.

5.2. Warm versus low-temperature operation

Here, the fuel consumption of the *low-temperature* operation will be compared with an ideal *warm* operation. The *warm* operation is defined as $T_\infty = 298.15$ K (25 °C), with T_∞ assumed constant along the entire driving cycle. At the beginning of the driving cycle $x_2 = T_\infty$ holds. Moreover, in the *warm operation*, the dynamics of the battery temperature is considered to be equal to zero; on the assumption that a cooling system is in place to keep $x_2 \approx 298.15$ K (25 °C) along the entire driving cycle. The offline-EMS is solved under *warm* operation conditions using the same vehicle parameters of the *low-temperature* operation. The fuel consumption for each operation is shown in Table 2. The *low-temperature* operation increases the fuel consumption with respect to the ideal *warm* operation in a 4.01%.

5.3. Comparison with DP

The optimal energy management for the low-temperature operation will be solved again using DP. The objective is to validate the optimality of the proposed approach and to benchmark its

Operation	Fuel consumption (WLTC-C3)	Difference
Warm	9.47 L/100 km	-
Low-temperature	9.85 L/100 km	+4.01 %

Table 2: Fuel consumption results for each operating condition.

computational efficiency. As mentioned in Section 1, DP has been widely used to solve the EMS in the literature of hybrid electric vehicles [11][12]. Its advantages are that it can solve the EMS with mixed input-state constraints and with a guarantee of global optimality. Its main drawback is that it has an exponential growth of memory and computational complexity with respect to the number of states, denoted as the *curse of dimensionality* [10]. For this reason, its use is limited to EMS formulations with one [11] or two states [13]. The DP algorithm is implemented using the Matlab code from [44], together with the iterative approach described in [45]. The results of the DP solution to (17) are displayed in Fig. 9 along with the solution computed with the proposed approach. The fuel consumption and computation times are compared in Table 3. The proposed approach is 46 times faster than DP but obtains +0.4% more fuel consumption as well. The small difference in fuel consumption can be due to the limited accuracy that DP posses as a consequence of the quantization of all variables and the Euler integration scheme in which it relies on.

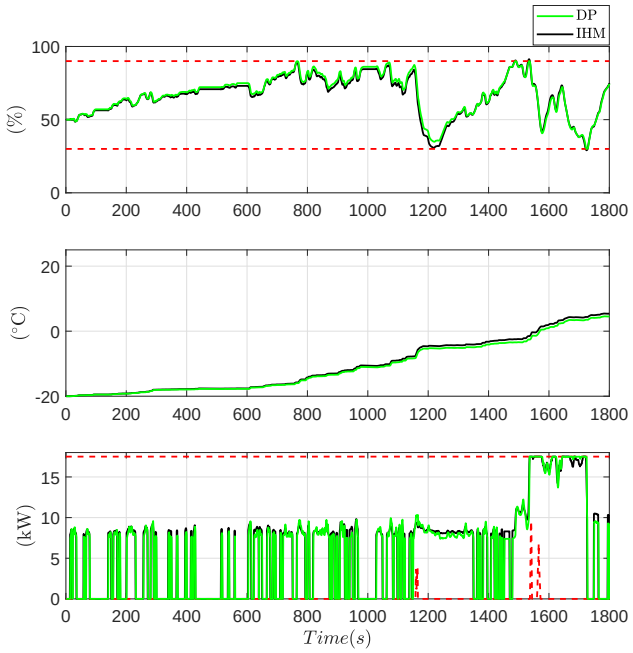

Figure 9: Solution to (17) for the *low-temperature* operation and the WLTC-C3 driving cycle with DP (green solid line) and the proposed implicit Hamiltonian minimization (black solid line). The dashed lines at the top and bottom subfigures represent the bounds on the state-of-energy and the control input, (17e) and (17d), respectively.

Method	Fuel DP (WLTC-C3)	Computation time (s)	Difference
DP	9.81 L/100 km	$6.187 \cdot 10^4$	-
Implicit Hamiltonian minimization	9.85 L/100 km	$1.319 \cdot 10^3$	+ 0.4 %

Table 3: Fuel consumption and computation time for DP and the proposed implicit Hamiltonian minimization under *low-temperature* conditions.

6. Conclusion

An indirect-approach method to compute the optimal offline EMS of a hybrid vehicle with several continuous states and under input and state constraints has been proposed. The indirect-approach method relies on exterior penalty functions and an implicit Hamiltonian minimization to handle the constraints and solve the PMP optimality conditions. A continuation procedure and a domain function-extension are also proposed to deal with the difficulties of computing a numerical solution. The proposed method does not require any *a priori* knowledge on the optimal solution and can be applied to EMS formulations with several inputs and states.

The proposed method is shown effective by solving the offline EMS of a hybrid vehicle under *low-temperature* conditions modeled as a two-state, the battery state-of-energy and temperature, mixed input-state constrained problem. The optimality of the solution is validated by obtaining an slightly different solution via DP. The small difference is not surprising since in DP all variables are quantized, which limits the accuracy of the solution. Moreover, the proposed method shows to be up to 46 times faster than DP.

One possible extension of this work is to apply it to a more general EMS formulation, for example, one that includes the engine and the catalytic converter temperature in order to include the emission of pollutants in its objective function [2, 46]. Another possible extension is to derive a real-time EMS approach based on a model predictive control scheme. The concept of an MPC scheme based on a stochastic prediction model and the solution of the BVP obtained from the PMP has been already explored in the literature [47].

Appendix A. Function extension with multiple variables

Let us consider $f_i \in X_i \subset \mathbb{R}^{n_i}$, where X_i is a convex region and f_i is C^∞. The Taylor series expansion of f_i around of $\tilde{x}$ is defined as follows:

$$\begin{aligned} f_i(x) =& f_i(\tilde{x}) + (x-\tilde{x})^T \nabla f_i(\tilde{x}) + \\ &+ \frac{1}{2}(x-\tilde{x})^T \nabla^2 f_i(\tilde{x})(x-\tilde{x}) + \dots \end{aligned}$$

With ∇f_i and $\nabla^2 f_i$ defined as the gradient and Hessian matrix of f_i, respectively. Given $\tilde{x} \in \partial X_i$, and $y \notin X$, the domain of f_i is extended outside X_i by the following function:

$$g_i(y) = f_i(\tilde{x}) + (y-\tilde{x})^T \nabla f_i(\tilde{x}) + \frac{1}{2}(y-\tilde{x})^T \nabla^2 f_i(\tilde{x})(y-\tilde{x}), \tag{A.1}$$

where $\tilde{x}$ is defined as the closest point on the boundary of X_i, ∂X_i, with respect to y.

Appendix B. Piecewise polynomial approximation of the the power demand and the On/Off signal command

The time derivatives of the power demand, $\dot{w}(t)$, and the On/Off command of the APU, $\dot{\vartheta}(t)$, are necessary to compute the optimal control dynamics $\dot{u}^*(t)$, see (33e). Since these signals are not available, a monotone piecewise cubic interpolation [48] is applied to $w(t)$ and $\vartheta(t)$ in order to approximate them. The interpolating polynomials of $w(t)$ and $\vartheta(t)$, denoted as $p_w(t)$ and $p_\vartheta(t)$, respectively, are guaranteed to be at least once continuously differential. The difference between the signals and its piecewise cubic approximations can be arbitrarily reduced by increasing the number of interpolating points at the cost of a greater computational effort.

The computation of the interpolating polynomials is carried out using a predefined Matlab function: *pchip*. Once $p_w(t)$ and $p_\vartheta(t)$ have been computed, $\dot{p}_w(t)$ and $\dot{p}_\vartheta(t)$ are used to approximate $\dot{w}(t)$ and $\dot{\vartheta}(t)$, respectively.

Acknowledgment

The present research was supported by the Regional Delegation for Research and Technology, the French Ministry of Higher Education and Research, and the National Center for Scientific Research. It was also supported by the ELSAT2020 project, co-funded by the European Regional Development Fund, the French state and the Hauts de France Region Council. The authors greatly acknowledge these institutions for their support.

References

[1] L. Guzzella and A. Sciarretta, *Vehicle Propulsion Systems: Introduction to Modeling and Optimization*. Springer Science & Business Media, 2012.

[2] D. Kum, H. Peng, and N. K. Bucknor, "Optimal energy and catalyst temperature management of plug-in hybrid electric vehicles for minimum fuel consumption and tail-pipe emissions," *IEEE Transactions on Control Systems Technology*, vol. 21, no. 1, pp. 14–26, 2013.

[3] P. Michel, A. Charlet, G. Colin, Y. Chamaillard, G. Bloch, and C. Nouillant, "Optimizing fuel consumption and pollutant emissions of gasoline-HEV with catalytic converter," *Control Engineering Practice*, vol. 61, pp. 198–205, 2017.

[4] D. F. Opila, X. Wang, R. McGee, R. B. Gillespie, J. A. Cook, and J. W. Grizzle, "An energy management controller to optimally trade off fuel economy and drivability for hybrid vehicles," *IEEE Transactions on Control Systems Technology*, vol. 20, no. 6, pp. 1490–1505, 2012.

[5] T. Miro-Padovani, G. Colin, A. Ketfi-Chérif, and Y. Chamaillard, "Implementation of an energy management strategy for hybrid electric vehicles including drivability constraints," *IEEE Transactions on Vehicular Technology*, vol. 65, no. 8, pp. 5918–5929, 2016.

[6] S. Ebbesen, P. Elbert, and L. Guzzella, "Battery state-of-health perceptive energy management for hybrid electric vehicles," *IEEE Transactions on Vehicular technology*, vol. 61, no. 7, pp. 2893–2900, 2012.

[7] A. Sciarretta, D. di Domenico, P. Pognant-Gros, and G. Zito, "Optimal energy management of automotive battery systems including thermal dynamics and aging," in *Optimization and Optimal Control in Automotive Systems*. Springer, 2014, pp. 219–236.

[8] C. Hou, M. Ouyang, L. Xu, and H. Wang, "Approximate pontryagins minimum principle applied to the energy management of plug-in hybrid electric vehicles," *Applied Energy*, vol. 115, pp. 174–189, 2014.

[9] E. Silvas, T. Hofman, N. Murgovski, L. P. Etman, and M. Steinbuch, "Review of optimization strategies for system-level design in hybrid electric vehicles," *IEEE Transactions on Vehicular Technology*, vol. 66, no. 1, pp. 57–70, 2016.

[10] R. E. Bellman, "Dynamic Programming," 1957.

[11] C.-C. Lin, H. Peng, J. W. Grizzle, and J.-M. Kang, "Power management strategy for a parallel hybrid electric truck," *IEEE Transactions on Control Systems Technology*, vol. 11, no. 6, pp. 839–849, 2003.

[12] S. Ebbesen, C. Dönitz, and L. Guzzella, "Particle swarm optimisation for hybrid electric drive-train sizing," *International Journal of Vehicle Design*, vol. 58, no. 2-4, pp. 181–199, 2012.
[13] M. Ansarey, M. S. Panahi, H. Ziarati, and M. Mahjoob, "Optimal energy management in a dual-storage fuel-cell hybrid vehicle using multi-dimensional dynamic programming," *Journal of Power Sources*, vol. 250, pp. 359–371, 2014.
[14] Y. Zhu, Y. Chen, G. Tian, H. Wu, and Q. Chen, "A four-step method to design an energy management strategy for hybrid vehicles," in *Proceedings of the 2004 American control conference*, vol. 1. IEEE, 2004, pp. 156–161.
[15] Z. Khalik, G. Padilla, T. Romijn, and M. Donkers, "Vehicle energy management with ecodriving: A sequential quadratic programming approach with dual decomposition," in *2018 Annual American Control Conference (ACC)*. IEEE, 2018, pp. 4002–4007.
[16] M. Pourabdollah, E. Silvas, N. Murgovski, M. Steinbuch, and B. Egardt, "Optimal sizing of a series PHEV: Comparison between convex optimization and particle swarm optimization," *IFAC-PapersOnLine*, vol. 48, no. 15, pp. 16–22, 2015.
[17] T. C. J. Romijn, M. Donkers, J. T. Kessels, and S. Weiland, "A distributed optimization approach for complete vehicle energy management," *IEEE Transactions on Control Systems Technology*, no. 99, pp. 1–17, 2018.
[18] E. D. Tate and S. P. Boyd, "Finding ultimate limits of performance for hybrid electric vehicles," SAE Technical Paper, Tech. Rep., 2000.
[19] M. Pourabdollah, N. Murgovski, A. Grauers, and B. Egardt, "Optimal sizing of a parallel PHEV powertrain," *IEEE Transactions on Vehicular Technology*, vol. 62, no. 6, pp. 2469–2480, 2013.
[20] P. Riedinger, C. Iung, and F. Kratz, "An optimal control approach for hybrid systems," *European Journal of Control*, vol. 9, no. 5, pp. 449–458, 2003.
[21] V. Ngo, T. Hofman, M. Steinbuch, and A. Serrarens, "Optimal control of the gearshift command for hybrid electric vehicles," *IEEE Transactions on Vehicular Technology*, vol. 61, no. 8, pp. 3531–3543, 2012.
[22] S. Delprat, T. Hofman, and S. Paganelli, "Hybrid vehicle energy management: Singular optimal control," *IEEE Transactions on Vehicular Technology*, vol. 66, no. 11, pp. 9654–9666, 2017.
[23] T. van Keulen, J. Gillot, B. de Jager, and M. Steinbuch, "Solution for state constrained optimal control problems applied to power split control for hybrid vehicles," *Automatica*, vol. 50, no. 1, pp. 187–192, 2014.
[24] T. Kareemulla, S. Delprat, and L. Czelecz, "State constrained hybrid vehicle optimal energy management: an interior penalty approach," *IFAC-PapersOnLine*, vol. 50, no. 1, pp. 10 040–10 045, 2017.
[25] J. Han, A. Sciarretta, and N. Petit, "Handling state constraints in fast-computing optimal control for hybrid powertrains," *IFAC-PapersOnLine*, vol. 50, no. 1, pp. 4781–4786, 2017.
[26] M. Sanchez and S. Delprat, "Hybrid vehicle energy management: Avoiding the explicit hamiltonian minimization," in *2018 IEEE Vehicle Power and Propulsion Conference (VPPC)*. IEEE, 2018, pp. 1–5.
[27] J. Ruan, P. D. Walker, P. A. Watterson, and N. Zhang, "The dynamic performance and economic benefit of a blended braking system in a multi-speed battery electric vehicle," *Applied energy*, vol. 183, pp. 1240–1258, 2016.
[28] T. M. Padovani, M. Debert, G. Colin, and Y. Chamaillard, "Optimal energy management strategy including battery health through thermal management for hybrid vehicles," *IFAC Proceedings Volumes*, vol. 46, no. 21, pp. 384–389, 2013.
[29] J. Jaguemont, L. Boulon, and Y. Dubé, "Characterization and modeling of a hybrid-electric-vehicle lithium-ion battery pack at low temperatures," *IEEE Transactions on Vehicular Technology*, vol. 65, no. 1, pp. 1–14, 2016.
[30] X. Lin, H. E. Perez, J. B. Siegel, A. G. Stefanopoulou, Y. Li, R. D. Anderson, Y. Ding, and M. P. Castanier, "Online parameterization of lumped thermal dynamics in cylindrical lithium ion batteries for core temperature estimation and health monitoring," *IEEE Transactions on Control Systems Technology*, vol. 21, no. 5, pp. 1745–1755, 2013.
[31] Z. Yang, D. Patil, and B. Fahimi, "Electrothermal modeling of lithium-ion batteries for electric vehicles," *IEEE Transactions on Vehicular Technology*, vol. 68, no. 1, pp. 170–179, 2019.
[32] N. Murgovski, L. Johannesson, J. Hellgren, B. Egardt, and J. Sjöberg, "Convex optimization of charging infrastructure design and component sizing of a plug-in series hev powertrain," *IFAC Proceedings Volumes*, vol. 44, no. 1, pp. 13 052–13 057, 2011.
[33] L. Lasdon, A. Waren, and R. Rice, "An interior penalty method for inequality constrained optimal control problems," *IEEE Transactions on Automatic Control*, vol. 12, no. 4, pp. 388–395, 1967.
[34] M. M. Lele and D. H. Jacobson, "A proof of the convergence of the Kelley-Bryson penalty function technique for state-constrained control problems," *Journal of Mathematical Analysis and Applications*, vol. 26, no. 1, pp. 163–169, 1969.
[35] D. E. Kirk, *Optimal control theory: an introduction*. Courier Corporation, 2012.

[36] D. S. Naidu, *Optimal control systems*. CRC press, 2002.
[37] G. M. Siouris, *An engineering approach to optimal control and estimation theory*. John Wiley & Sons, Inc., 1996.
[38] U. M. Ascher, R. M. Mattheij, and R. D. Russell, *Numerical solution of boundary value problems for ordinary differential equations*. Siam, 1994, vol. 13.
[39] J. Kierzenka and L. F. Shampine, "A BVP solver based on residual control and the Maltab PSE," *ACM Transactions on Mathematical Software*, vol. 27, no. 3, pp. 299–316, 2001.
[40] N. Petit and A. Sciarretta, "Optimal drive of electric vehicles using an inversion-based trajectory generation approach," *IFAC Proceedings Volumes*, vol. 44, no. 1, pp. 14 519–14 526, 2011.
[41] J. F. Bonnans and A. Hermant, "Second-order analysis for optimal control problems with pure state constraints and mixed control-state constraints," in *Annales de l'Institut Henri Poincare (C) Non Linear Analysis*, vol. 26, no. 2. Elsevier, 2009, pp. 561–598.
[42] B. C. Fabien, "Numerical solution of constrained optimal control problems with parameters," *Applied Mathematics and Computation*, vol. 80, no. 1, pp. 43–62, 1996.
[43] K. Graichen and N. Petit, "Constructive methods for initialization and handling mixed state-input constraints in optimal control," *Journal Of Guidance, Control, and Dynamics*, vol. 31, no. 5, pp. 1334–1343, 2008.
[44] O. Sundstrom and L. Guzzella, "A generic dynamic programming matlab function," in *2009 IEEE control applications,(CCA) & intelligent control,(ISIC)*. IEEE, 2009, pp. 1625–1630.
[45] R. Luus, *Iterative dynamic programming*. Chapman and Hall/CRC, 2000.
[46] F. Merz, A. Sciarretta, J.-C. Dabadie, and L. Serrao, "On the optimal thermal management of hybrid-electric vehicles with heat recovery systems," *Oil & Gas Science and Technology–Revue dIFP Energies nouvelles*, vol. 67, no. 4, pp. 601–612, 2012.
[47] S. Xie, X. Hu, Z. Xin, and J. Brighton, "Pontryagins minimum principle based model predictive control of energy management for a plug-in hybrid electric bus," *Applied Energy*, vol. 236, pp. 893–905, 2019.
[48] F. N. Fritsch and R. E. Carlson, "Monotone piecewise cubic interpolation," *SIAM Journal on Numerical Analysis*, vol. 17, no. 2, pp. 238–246, 1980.